ARTICLES
https://doi.org/10.1038/s41565-018-0091-5
nature nanotechnology

# Spin–photon interface and spin-controlled photon switching in a nanobeam waveguide

Alisa Javadi[1*], Dapeng Ding[1], Martin Hayhurst Appel[1], Sahand Mahmoodian[1], Matthias Christian Löbl[2], Immo Söllner[2], Rüdiger Schott[3], Camille Papon[1], Tommaso Pregnolato[1], Søren Stobbe[1], Leonardo Midolo[1], Tim Schröder[1], Andreas Dirk Wieck[3], Arne Ludwig[2], Richard John Warburton[2] and Peter Lodahl[1*]

**The spin of an electron is a promising memory state and qubit. Connecting spin states that are spatially far apart will enable quantum nodes and quantum networks based on the electron spin. Towards this goal, an integrated spin–photon interface would be a major leap forward as it combines the memory capability of a single spin with the efficient transfer of information by photons. Here, we demonstrate such an efficient and optically programmable interface between the spin of an electron in a quantum dot and photons in a nanophotonic waveguide. The spin can be deterministically prepared in the ground state with a fidelity of up to 96%. Subsequently, the system is used to implement a single-spin photonic switch, in which the spin state of the electron directs the flow of photons through the waveguide. The spin–photon interface may enable on-chip photon–photon gates, single-photon transistors and the efficient generation of a photonic cluster state.**

Access to the electron spin is at the heart of many protocols for integrated and distributed quantum-information processing[1–3]. For instance, interfacing the spin state of an electron and a photon can be utilized to perform quantum gates between photons[2,4] or to entangle remote spin states[5–8]. Ultimately, a quantum network of entangled spins constitutes a new paradigm in quantum optics[1].

Solid-state quantum emitters embedded in planar nanostructures offer a scalable route to integrated light–matter interfaces[7,9]. Among these emitters, InGaAs quantum dots are arguably the most-developed platform. Quantum dots have been integrated in various nanostructures with near-unity coupling efficiencies[10–12]. Such a high coupling efficiency has enabled near-deterministic and indistinguishable single-photon sources[13,14], as well as single-photon level nonlinearities[15,16]. Furthermore, chiral light–matter interaction that leads to directional photon emission and scattering[17–19] has opened new prospects for integrated quantum-information processing[20].

Significant progress has been made on the coherent control of the spin state of electrons and holes in quantum dots[21–25], spin–photon entanglement and spin–spin entanglement[5]. Transferring the performance to highly efficient photon-emitter interfaces implemented in photonic nanostructures is not a trivial task, and pioneering experiments have considered primarily narrow-linewidth cavities[26–29] and external in-plane magnetic fields, which do not require a long spin lifetime[30]. In comparison, a waveguide geometry offers a broadband operation[9] whereby two stable ground-state spins can simultaneously be coupled well to a single optical mode. This allows a long-lived spin memory to be combined with an efficient photon-emitter interface. Moreover, access to chiral interaction between the optical mode and the spin state enables a number of promising features, such as non-reciprocal devices[17,18].

In the present work, we demonstrate an efficient interface between the spin state of an electron in a quantum dot and the optical mode of a nanobeam waveguide. Based on this system, we realize a proof-of-concept optically programmable photon switch that is controlled by the spin state of the quantum dot. We achieve a deterministic charging of the quantum dot, whereby high-fidelity optical spin-state preparation is obtained with an external magnetic field applied parallel to the quantum-dot growth axis (Faraday geometry). We observe a spin lifetime of $T_1 \approx 4\,\mu s$ and a diagonal decay rate ($\gamma$) that is two orders of magnitude smaller than the vertical decay rate ($\Gamma$), $\Gamma \simeq 100\gamma$. Figure 1a gives the level structure. Together with the long spin lifetime, $T_1 \simeq 50\gamma^{-1}$, this is the favourable condition for realizing a high-fidelity and long-lived spin-state preparation[23], as required for photon–photon gates and single-photon transistors[2,31]. Indeed, we experimentally demonstrate a spin-preparation fidelity that approaches 96%. Also, we show that the quantum-dot spin controls transmission through the waveguide and the optical control of the spin enables the transmission to be turned on and off. Finally, we demonstrate that the spin–photon interaction is chiral, which may be used to implement non-reciprocal light transport[18] as a basis for novel quantum photonic devices, such as on-chip single-photon circulators[32], integrated isolators or building blocks for distributed quantum networks[33].

## Level structure

Figure 1a shows the level structure of a negatively charged quantum dot under the influence of a static magnetic field along the growth axis ($B_z$) (ref. [23]). In the ground state, the spin of the trapped electron is oriented parallel or antiparallel to the growth axis, which are labeled as spin-up ($|\uparrow\rangle$) and spin-down states ($|\downarrow\rangle$), respectively. The two excited states are negatively charged excitons ($X^-$), and consist of two spin-paired electrons and a single hole. The vertical transitions are circularly polarized ($\sigma_+$ and $\sigma_-$). The diagonal transitions are weakly allowed because of the in-plane Overhauser field and heavy-hole–light-hole mixing in the valence band of the quantum dot, with the latter being the dominant mechanism at higher magnetic fields[34].

[1]Niels Bohr Institute, University of Copenhagen, Copenhagen, Denmark. [2]Department of Physics, University of Basel, Basel, Switzerland. [3]Lehrstuhl für Angewandte Festkörperphysik, Ruhr-Universität Bochum, Bochum, Germany. *e-mail: javadi@nbi.ku.dk; lodahl@nbi.ku.dk



© 2018 Macmillan Publishers Limited, part of Springer Nature. All rights reserved.

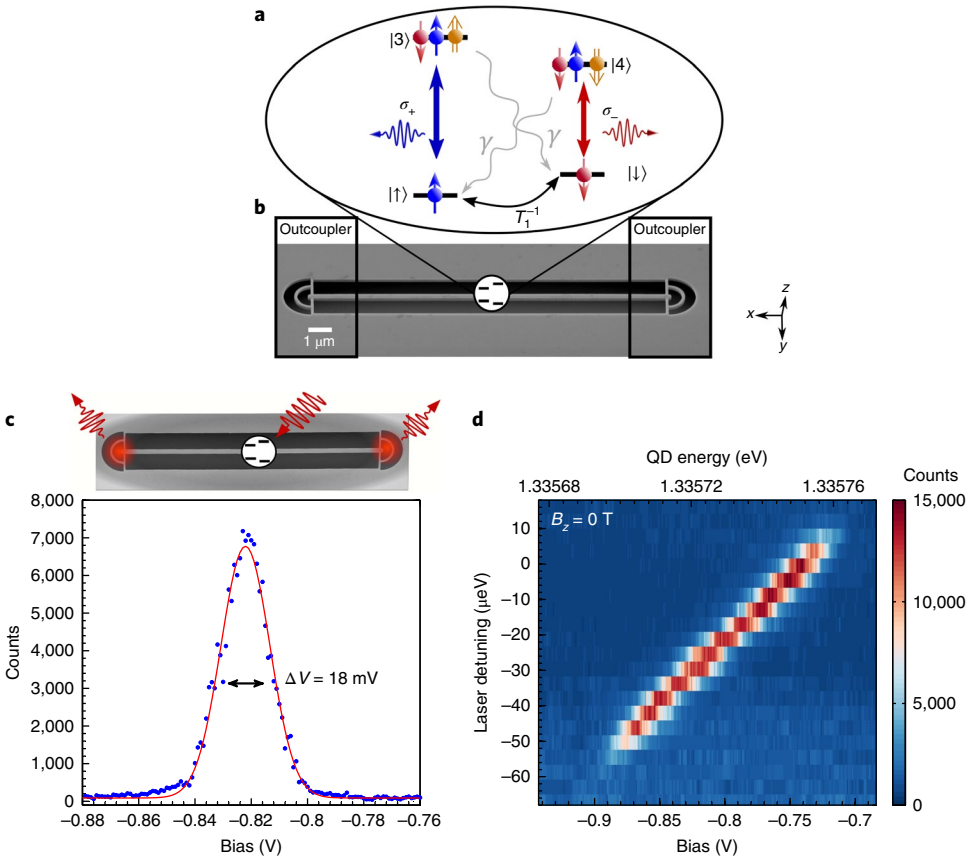



**Fig. 1 | Resonant spectroscopy of a negatively charged quantum dot in a nanophotonic waveguide. a**, Level structure of a negatively charged quantum dot. The $|\uparrow\rangle$ and $|\downarrow\rangle$ ground states correspond to spin quantum numbers $m_j = +\frac{1}{2}$ and $m_j = -\frac{1}{2}$. A magnetic field ($B_z$) along the growth axis (Faraday geometry) splits the two ground states. The diagonal transitions are inhibited because of optical selection rules, but weakly allowed due to heavy-hole–light-hole mixing. $\gamma$ is a spontaneous decay rate through the diagonal transition, $T_1$ is the ground-state lifetime and $\sigma_+$ ($\sigma_-$) indicate a right- (left-)hand circularly polarized dipole transition. **b**, SEM of a nanobeam waveguide. The quantum dot is located close to the centre of the waveguide and an electric field is applied across the quantum dot using a diode structure. **c**, Resonance fluorescence from $X^-$ under resonant excitation at $B_z = 0$ T. The quantum dot is excited from the top of the waveguide with cross-polarized light at an energy indicated by the black arrow. The emission is collected from the gratings and the quantum dot is tuned through the resonance by varying the bias voltage. The solid curve is a Gaussian fit with a linewidth (full-width at half-maximum) of $\Delta V = 18$ mV, which corresponds to $\Delta E = 7.4$ μeV. **d**, Plateau map at $B_z = 0$ T. Resonance fluorescence from the $X^-$ exciton is plotted as a function of the laser energy and the applied bias voltage. The top axis shows the energy of the $X^-$ transition.

## Sample design and characterization

Figure 1b shows a scanning electron micrograph (SEM) of a nanobeam waveguide, terminated with grating outcouplers at the two ends. A layer of InGaAs quantum dots is positioned in the centre of the membrane inside a p–i–n–i–n diode grown along the $z$ direction[35]. The design of the diode facilitates deterministic charging of the quantum dot as well as tuning of its energy levels by applying a bias voltage (Supplementary Sections I and II give details of the sample design and its electrical characteristics).

The plot in Fig. 1c shows emission from $X^-$ under a weak resonant excitation at $B_z = 0$ T as a function of the bias voltage. The laser is fixed at 1.3352 eV and the energy of the quantum-dot transition is tuned by changing the bias voltage. The linewidth of the resonance is 7.4 eV (~9× the natural linewidth), with the broadening attributed to charge noise from the environment of the quantum dot[36], although not a fundamental limitation in nanobeam waveguides in which narrow linewidth quantum dots were recently observed[14]. Figure 1d shows a plateau map of the resonance fluorescence from the $X^-$ transition as a function of excitation laser energy and the bias voltage. The relevant transition-energy range is between 1.335696 eV and 1.335760 eV, in which the quantum dot is charged with a single electron in the ground state. Below this plateau region the quantum dot is empty and above it the quantum dot is charged with two electrons and hence the fluorescence from $X^-$ vanishes[37]. In the centre of the plateau, the single-electron charged state of the quantum dot is a stable state, and the spin state of the electron is only influenced by second-order processes, such as co-tunnelling with the back contact[34,38] or by Auger recombination[39].

## Preparation of the optical spin state

To prepare two optically accessible spin ground states with an energy difference larger than the transition linewidth, we lift the degeneracy by inducing a Zeeman shift at $B_z = 0.55$ T. We probe the $|\uparrow\rangle$ and $|\downarrow\rangle$ states through resonance fluorescence from the $X^-$ exciton. Figure 2a shows the plateau map of the $X^-$ exciton. The emission plateau (regions A and B) originates from the high-energy (blue) transition of the negatively charged exciton, whereas region C corresponds to emission from the low-energy (red) transition. The blue transition is ~4 times brighter than the red transition, which is due to a chiral light–matter interaction[18–20] (Supplementary Section III gives a detailed analysis). At the central part of the plateau, region B, optical spin pumping takes place and the emission from $X^-$ is suppressed due to spin-non-conserving diagonal transitions. At the edges of the plateaus, region A, the electron is strongly coupled to



© 2018 Macmillan Publishers Limited, part of Springer Nature. All rights reserved.

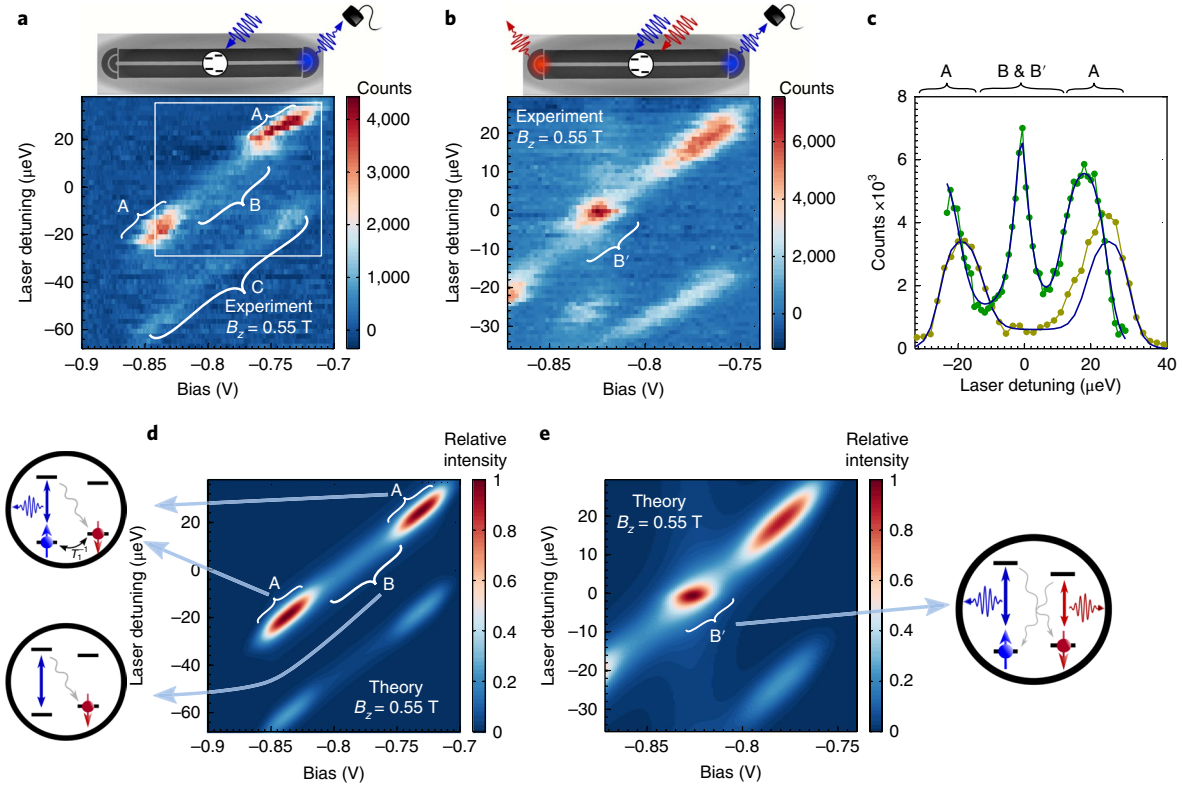



**Fig. 2 | Quantum dot spin preparation in a nanophotonic waveguide. a**, Plateau map of the $X^-$ transitions at $B_z = 0.55$ T. The plateau regions A and B correspond to fluorescence from the blue transition in Fig. 1a, whereas the region marked as C corresponds to emission from the red transition in Fig. 1a. The two plateaus have different intensities due to chiral light–matter interaction. The central part of the plateau is dim, due to optical spin pumping from the $|\uparrow\rangle$ state to the $|\downarrow\rangle$ state and vice versa. At the edges of the plateau (region A), spin pumping is suppressed due to co-tunnelling between the electron in the quantum dot and the Fermi sea in the back contact. **b**, Same as in **a** with a second laser fixed at −40 eV, which corresponds to the centre of the $|\downarrow\rangle$ plateau. The bright spot in the centre (B′) is caused by simultaneous excitation of the blue and red transitions, when the first laser is tuned to the centre of the plateau of the blue transition. The plotted range corresponds to the white box in **a**. The resonance voltages are shifted by 50 mV due to charge-screening effects induced by the second laser. **c**, Linecuts through the top plateau in **a** and **b**, coloured as yellow and green, respectively. The solid curves are theoretical fits to the data. **d**,**e**, Theoretical models of the plateau maps in **a** and **b**, respectively. Supplementary Section IV gives details of the modelling. By modelling the data in **a**, we extract the spin lifetime *of* $T_1 = 3.8 \pm 1.2\,\mu$s.

the Fermi sea in the back contact and its spin is randomized over short timescales (about tens of nanoseconds)[34,38], which hinders spin pumping. At these points, the fluorescence is ~6–7 times brighter than in the centre (linecut data in Fig. 2c). By comparing the resonance fluorescence intensity at the edge of the plateau with the emission at the centre of the plateau, we extract a lower bound on the spin-preparation fidelity $\langle\downarrow|\rho|\downarrow\rangle \geq 86\%$ for the data in Fig. 2a, where $\rho$ is the density matrix of the prepared state (Supplementary Section IV gives details of the model and the related data analysis). Supplementary Section VII presents a detailed study of the spin-preparation fidelity as a function of the laser power and the applied magnetic field. At higher magnetic fields and laser powers, we achieve fidelities up to $\langle\downarrow|\rho|\downarrow\rangle = 96\%$.

To confirm the optical spin pumping, we performed a two-colour resonance fluorescence experiment[40] in which one laser is fixed at the centre of the plateau of the red transition as the frequency of the second laser is scanned. Figure 2b shows the two-colour plateau map of the $X^-$ exciton. When the two lasers are on resonance with the blue and red transitions simultaneously, B′, they cancel each others' spin-pumping effect and the resonance fluorescence from the quantum dot is recovered. Figure 2d,e depicts the theoretical model of the data (Supplementary Section IV gives details of the model). The experimental behaviour is quantitatively described by the theory, for $T_1 = 3.8 \pm 1.2\,\mu$s. We also extract $\gamma = 13 \pm 1$ MHz using time-resolved measurements (details are described in Supplementary Section V). $T_1$ may also be extracted directly by pump–delay–probe experiments from which we obtain $T_1 = 4.3 \pm 0.2\,\mu$s (details are given in Supplementary Section VI). These results are in very good agreement with the parameters extracted from modelling the data (Fig. 2a). A longer spin lifetime has been reported for quantum dots in a bulk medium[22]. Potentially, the influence of surface currents or dangling bonds at the surfaces may reduce the lifetime in photonic nanostructures. Importantly, we emphasize that the observed spin lifetime in this experiment exceeds the longest spin-coherence time reported with quantum dots[41], even after implementing spin–echo techniques[24]. Consequently, the reported $T_1$ is sufficiently long to enable quantum applications.

## Spin-controlled photon switching

A quantum emitter coupled to a single optical mode can modify the light-transmission properties significantly[15,31]. For an efficient coupling, this interaction can be sensitive at the single-photon level. The colour map in Fig. 3a shows the normalized transmission of a weak probe as a function of its energy and the bias voltage of the diode at $B_z = 0$ T. When the probe is on resonance with the $X^-$ transition, the transmission of the probe is reduced due to the interaction with the transition[15], where the quantum dot scatters one photon at a time. This is observed as a dip in the plateau map in Fig. 3a. We observe a maximum contrast of 15% in the transmission, which is mainly limited by the inhomogeneous broadening of the quantum-dot transition.



© 2018 Macmillan Publishers Limited, part of Springer Nature. All rights reserved.

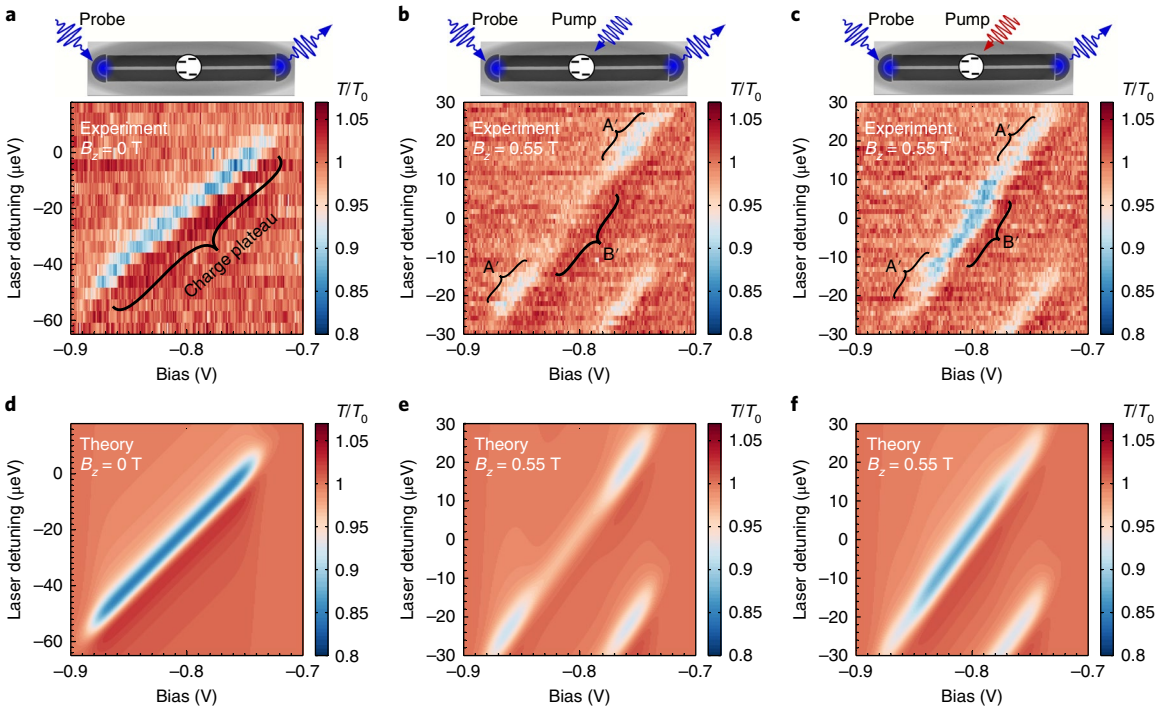



**Fig. 3 | Spin-controlled resonant transmission through the nanophotonic waveguide. a**, Measurement of the transmission through the waveguide as a function of the probe-pulse energy and the bias voltage at $B_z = 0$ T. A weak probe pulse is launched into the waveguide through the grating on the left-hand side and the transmission is monitored. When the probe is on resonance with the quantum-dot transition, the scattering from the quantum dot reduces the transmission of the probe. The probe power is set an order of magnitude below the saturation power of the quantum dot. **b**,**c**, Pump–probe measurements at $B_z = 0.55$ T as the probe is swept along the charge plateau of the blue transition. A resonant pump laser launched from the top of the waveguide prepares the spin state of the electron during the pump cycle. The detuning between the probe and pump is fixed to 0 eV for **b** and 40 eV for **c**. In **b**, the spin state of the electron is prepared in the $|\downarrow\rangle$ state during the pump cycle. As a result, the blue transition is turned off, and the transmission of the probe is maximized. A′ indicates the edges of the charge plateau at which co-tunnelling is strong. In **c**, the pump laser prepares the electron spin in the $|\uparrow\rangle$ state, and the blue transition reduces the transmission of the probe. **d**–**f**, Theoretical models of the experiments in **a**–**c**. Supplementary Section IV gives the details of the models.

To implement a spin-state-dependent interaction between the quantum dot and the waveguide mode, we use optical spin pumping to prepare deterministically the spin state of the quantum dot. We use optical pulses for spin preparation and readout, as this is eventually required to turn the switch on and off. A strong laser pulse (pump) with a duration of 1 s incident from the top of the waveguide prepares the spin state of the electron. Subsequently, a weak pulse (probe) with a duration of 200 ns, coupled in and out via the gratings, probes the single-photon transmission through the waveguide. Figure 3b shows the normalized transmission through the waveguide when the probe and pump pulses are on resonance. In the centre of the plateau, B′, the pump pulse prepares the spin of the electron in the $|\downarrow\rangle$ state with a high fidelity. This state is off resonance with the probe and hence the transmission recovers to the level $T_0$, which is the level encountered when the probe is far from resonance of the quantum-dot transition. At the edges of the plateau, A′, the transmission of the probe is reduced due to inefficient spin-state preparation. Figure 3c shows the transmission of the waveguide as the pump laser is detuned by −40 μeV from the probe. In this case, the pump prepares the spin of the electron in the $|\uparrow\rangle$ state, which is on resonance with the probe. As a result, the probe pulse interacts with the blue transition of the $X^-$ exciton. At the centre of the plateau, B′, the transmission of the waveguide is reduced to 0.87, similar to the value found without an external magnetic field.

The ability to prepare a spin deterministically and thereby control the waveguide transmission constitutes a proof-of-concept realization of a switch for single photons. The on and off states of the switch correspond to the spin of the electron prepared in the $|\downarrow\rangle$ and $|\uparrow\rangle$ states, respectively. The transmission can be switched by tuning the pump pulse to either the red or the blue transition of the quantum dot. The green curve in Fig. 4a shows transmission through the waveguide with the probe laser fixed at the centre of the blue plateau and the spin state of the electron prepared in the $|\uparrow\rangle$ state, which corresponds to the off state of the switch. The yellow dataset corresponds to the case in which the switch is initialized in the on state. In the off state, the quantum dot blocks ~12% of the probe light. Figure 4b shows the contrast of the transmission through the waveguide as a function of the energy detuning of the probe laser from the centre of the blue plateau. The contrast is defined as the modulation of the transmission through the waveguide as a result of the interaction of the laser with the quantum-dot transition (Fig. 4a gives a visual representation). We observe a switching ratio of more than a factor of four between on and off states, which could be improved further by reducing the spectral diffusion due to residual charge noise broadening. Ultimately, the switch could be operated in a genuine quantum regime if the spin was initially prepared in a coherent superposition state. Such a quantum switch could create a photonic Schrödinger cat state when applied to a weak coherent state[31].

It is instructive to benchmark the reported performance of all-optical switching. The pump power on the sample for the data in Fig. 4 is around 40 nW for a duration of 1 s, which corresponds to 40 fJ per pump cycle. During each switching cycle the quantum dot scatters $\Gamma/\gamma$ photons, which is about 100 photons for the measurements reported here[31]. This energy could be further reduced by up to two orders of magnitude by directly launching the pump pulse inside



© 2018 Macmillan Publishers Limited, part of Springer Nature. All rights reserved.

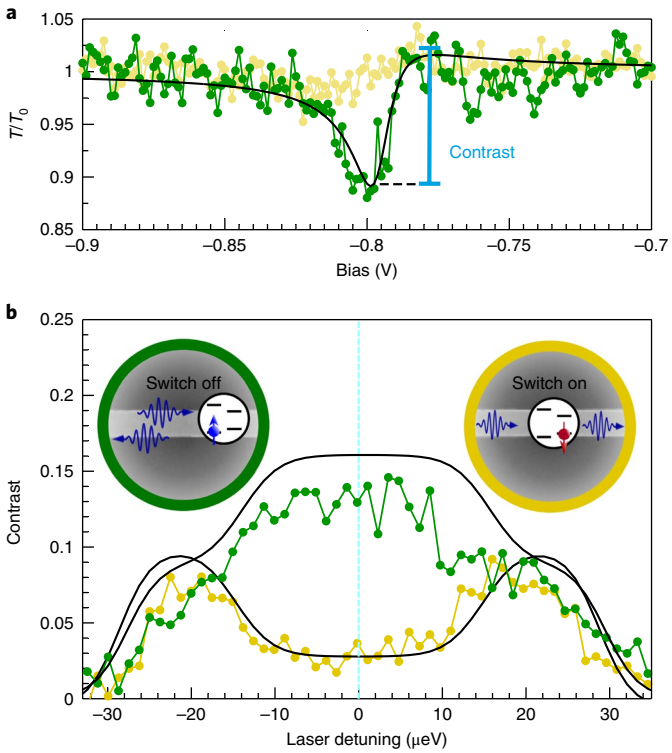



**Fig. 4 | Spin-controlled switching of the transmission. a**, Transmission through the waveguide as a function of the bias voltage at the centre of the blue plateau. The yellow and green data correspond to transmission through the waveguide as the electron spin is initialized in $|\downarrow\rangle$ or $|\uparrow\rangle$, respectively. **b**, Contrast in the transmission through the waveguide along the charge plateau as a function of the detuning of the laser from the centre of the blue plateau. The top left inset is a schematic demonstration of the reflection of photons by the quantum dot when the spin of the electron is prepared in the $|\uparrow\rangle$ state, and corresponds to the green data points. The right-hand inset shows the case in which the spin of the electron is prepared in $|\downarrow\rangle$ and the quantum dot does not interact with the probe. From the data in this figure we infer a switching contrast ratio of four. The data correspond to linecuts through A′ and B′ regions in Fig. 3b (green) and Fig. 3c (yellow). The solid curves are theoretical models based on the parameters extracted from the resonance fluorescence experiments (Supplementary Section IV).

the waveguide. The switching time in the present work is slower than in previous demonstrations based on the strong coupling of a quantum-dot exciton transition to a cavity[42,43]. However, once programmed, the switch retains its state for up to 4 μs. As a comparison, switches based on a strong coupling decay after 50 ps (refs [42,43]) and switches based on material nonlinearities operate on a similar timescale[44,45]. In the present work, we demonstrate switching in a system that can simultaneously offer access to a long-lived quantum memory in the form of the ground-state electron spin, which is a prerequisite for many quantum-information applications[46].

We have demonstrated an all-optical control of a single electron spin in a quantum dot efficiently coupled to a nanophotonic waveguide. Based on this approach, a single spin controls the flow of photons through the waveguide. The work opens a range of new opportunities in quantum optics to exploit deterministic photon–spin coupling, for example, to generate long strings of photonic cluster states[47], a high-fidelity photon–photon gate[2] or single-photon transistors[31], where the spin state of the electron may be coherently controlled either with microwave pulses[48] or by utilizing the weak diagonal transitions[49]. Extending to the coupling of two quantum dots would enable us to construct a fundamental building block for a distributed photonic quantum network[33]. For these potential applications, it is favourable to work in the Faraday geometry (external magnetic field along the growth direction), as is the case here, because the operation fidelity scales as $\sim 1-\gamma/\Gamma$ (ref. [31]), where $\Gamma \gg \gamma$ as reported here. One challenge, however, is the coupling of the electron spin to the noisy nuclear bath that leads to electron-spin dephasing. Recent work has demonstrated how to reduce significantly the noise on the Overhauser field by feedback control of the nuclear ensemble[50,51].

**Data availability.** The data that support the plots within this paper and other findings of this study are available from the corresponding authors on reasonable request.

Received: 25 August 2017; Accepted: 9 February 2018;
Published online: 19 March 2018

## References

1. Kimble, H. J. The quantum internet. *Nature* **453**, 1023–1030 (2008).
2. Duan, L. M. & Kimble, H. J. Scalable photonic quantum computation through cavity-assisted interactions. *Phys. Rev. Lett.* **92**, 127902 (2004).
3. Van Meter, R., Ladd, T. D., Fowler, A. G. & Yamamoto, Y. Distributed quantum computation architecture using semiconductor nanophotonics. *Int. J. Quantum Inf.* **8**, 295–323 (2010).
4. Hacker, B., Welte, S., Rempe, G. & Ritter, S. A photon–photon quantum gate based on a single atom in an optical resonator. *Nature* **536**, 193–196 (2016).
5. Delteil, A. et al. Generation of heralded entanglement between distant hole spins. *Nat. Phys.* **12**, 218–223 (2016).
6. Hucul, D. et al. Modular entanglement of atomic qubits using photons and phonons. *Nat. Phys.* **11**, 37–42 (2015).
7. Sipahigil, A. et al. An integrated diamond nanophotonics platform for quantum-optical networks. *Science* **354**, 847–850 (2016).
8. Cirac, J. I., Zoller, P., Kimble, H. J. & Mabuchi, H. Quantum state transfer and entanglement distribution among distant nodes in a quantum network. *Phys. Rev. Lett.* **78**, 3221–3224 (1997).
9. Lodahl, P., Mahmoodian, S. & Stobbe, S. Interfacing single photons and single quantum dots with photonic nanostructures. *Rev. Mod. Phys.* **87**, 347–400 (2015).
10. Arcari, M. et al. Near-unity coupling efficiency of a quantum emitter to a photonic crystal waveguide. *Phys. Rev. Lett.* **113**, 093603 (2014).
11. Claudon, J. et al. A highly efficient single-photon source based on a quantum dot in a photonic nanowire. *Nat. Photon.* **4**, 174–177 (2010).
12. Makhonin, M. et al. Waveguide coupled resonance fluorescence from on-chip quantum emitter. *Nano Lett.* **14**, 6997–7002 (2014).
13. Ding, X. et al. On-demand single photons with high extraction efficiency and near-unity indistinguishability from a resonantly driven quantum dot in a micropillar. *Phys. Rev. Lett.* **116**, 020401 (2016).
14. Kiršanské, G. et al. Indistinguishable and efficient single photons from a quantum dot in a planar nanobeam waveguide. *Phys. Rev. B* **96**, 165306 (2017).
15. Javadi, A. et al. Single-photon non-linear optics with a quantum dot in a waveguide. *Nat. Commun.* **6**, 8655 (2015).
16. Bennett, A. et al. A semiconductor photon-sorter. *Nat. Nanotech.* **11**, 857–860 (2016).
17. Luxmoore, I. J. et al. Interfacing spins in an InGaAs quantum dot to a semiconductor waveguide circuit using emitted photons. *Phys. Rev. Lett.* **110**, 037402 (2013).
18. Söllner, I. et al. Deterministic photon-emitter coupling in chiral photonic circuits. *Nat. Nanotech.* **10**, 775–778 (2015).
19. Coles, R. et al. Chirality of nanophotonic waveguide with embedded quantum emitter for unidirectional spin transfer. *Nat. Commun.* **7**, 11183 (2016).
20. Lodahl, P. et al. Chiral quantum optics. *Nature* **541**, 473–480 (2017).
21. Kroutvar, M. et al. Optically programmable electron spin memory using semiconductor quantum dots. *Nature* **432**, 81–84 (2004).
22. Atatüre, M. et al. Quantum-dot spin-state preparation with near-unity fidelity. *Science* **312**, 551–553 (2006).
23. Warburton, R. J. Single spins in self-assembled quantum dots. *Nat. Mater.* **12**, 483–493 (2013).
24. Press, D. et al. Ultrafast optical spin echo in a single quantum dot. *Nat. Photon.* **4**, 367–370 (2010).
25. Stockill, R. et al. Quantum dot spin coherence governed by a strained nuclear environment. *Nat. Commun.* **7**, 12745 (2016).
26. Pinotsi, D., Fallahi, P., Miguel-Sanchez, J. & Imamoglu, A. Resonant spectroscopy on charge tunable quantum dots in photonic crystal structures. *IEEE J. Quant. Electron* **47**, 1371–1374 (2011).



© 2018 Macmillan Publishers Limited, part of Springer Nature. All rights reserved.

27. Carter, S. G. Quantum control of a spin qubit coupled to a photonic crystal cavity. *Nat. Photon.* **7**, 329–334 (2013).
28. Sweeney, T. M. et al. Cavity-stimulated Raman emission from a single quantum dot spin. *Nat. Photon.* **8**, 442–447 (2014).
29. Sun, S., Kim, H., Solomon, G. S. & Waks, E. A quantum phase switch between a single solid-state spin and a photon. *Nat. Nanotech.* **11**, 539–544 (2016).
30. Emary, C., Xu, X., Steel, D. G., Saikin, S. & Sham, L. J. Fast initialization of the spin state of an electron in a quantum dot in the Voigt configuration. *Phys. Rev. Lett.* **98**, 047401 (2007).
31. Chang, D. E., Sørensen, A. S., Demler, E. A. & Lukin, M. D. A single-photon transistor using nanoscale surface plasmons. *Nat. Phys.* **3**, 807–812 (2007).
32. Scheucher, M., Hilico, A., Will, E., Volz, J. & Rauschenbeutel, A. Quantum optical circulator controlled by a single chirally coupled atom. *Science* **354**, 1577–1580 (2016).
33. Mahmoodian, S., Lodahl, P. & Sørensen, A. S. Quantum networks with chiral-light–matter interaction in waveguides. *Phys. Rev. Lett.* **117**, 240501 (2016).
34. Dreiser, J. et al. Optical investigations of quantum dot spin dynamics as a function of external electric and magnetic fields. *Phys. Rev. B* **77**, 075317 (2008).
35. Löbl, M. C. et al. Narrow optical linewidths and spin pumping on charge-tunable, close-to-surface self-assembled quantum dots in an ultra-thin diode. *Phys. Rev. B* **96**, 165440 (2017).
36. Kuhlmann, A. V. et al. Charge noise and spin noise in a semiconductor quantum device. *Nat. Phys.* **9**, 570–575 (2013).
37. Warburton, R. J. et al. Optical emission from a charge-tunable quantum ring. *Nature* **405**, 926–929 (2000).
38. Smith, J. M. et al. Voltage control of the spin dynamics of an exciton in a semiconductor quantum dot. *Phys. Rev. Lett.* **94**, 197402 (2005).
39. Kurzmann, A., Ludwig, A., Wieck, A. D., Lorke, A. & Geller, M. Auger recombination in self-assembled quantum dots: quenching and broadening of the charged exciton transition. *Nano Lett.* **16**, 3367–3372 (2016).
40. Kroner, M. et al. Resonant two-color high-resolution spectroscopy of a negatively charged exciton in a self-assembled quantum dot. *Phys. Rev. B* **78**, 075429 (2008).
41. Wüst, G. et al. Role of the electron spin in determining the coherence of the nuclear spins in a quantum dot. *Nat. Nanotech.* **11**, 885–889 (2016).
42. Fushman, I. et al. Controlled phase shifts with a single quantum dot. *Science* **320**, 769–772 (2008).
43. Volz, T. et al. Ultrafast all-optical switching by single photons. *Nat. Photon.* **6**, 605–609 (2012).
44. Nozaki, K. et al. Sub-femtojoule all-optical switching using a photonic-crystal nanocavity. *Nat. Photon.* **4**, 477–483 (2010).
45. Miller, D. A. Are optical transistors the logical next step? *Nat. Photon.* **4**, 3–5 (2010).
46. Lodahl, P. Quantum-dot based photonic quantum networks. *Quantum Sci. Technol.* **3**, 013001 (2018).
47. Lindner, N. H. & Rudolph, T. Proposal for pulsed on-demand sources of photonic cluster state strings. *Phys. Rev. Lett.* **103**, 113602 (2009).
48. Kroner, M. et al. Optical detection of single-electron spin resonance in a quantum dot. *Phys. Rev. Lett.* **100**, 156803 (2008).
49. Hansom, J. et al. Environment-assisted quantum control of a solid-state spin via coherent dark states. *Nat. Phys.* **10**, 725–730 (2014).
50. Xu, X. et al. Optically controlled locking of the nuclear field via coherent dark-state spectroscopy. *Nature* **459**, 1105–1109 (2009).
51. Éthier-Majcher, G. et al. Improving a solid-state qubit through an engineered mesoscopic environment. *Phys. Rev. Lett.* **119**, 130503 (2017).


## Acknowledgements

We acknowledge N. J. Taba and C. L. Dreeßen for help during the initial stages of the measurements. We gratefully acknowledge financial support from the European Research Council (ERC Advanced Grant 'SCALE'), Innovation Fund Denmark (Quantum Innovation Center 'Qubiz') and the Danish Council for Independent Research. I.S., M.C.L. and R.J.W. acknowledge support from SNF (project 200020_156637) and NCCR QSIT. A.L. and A.D.W. gratefully acknowledge support of BMBF (Q.com-H 16KIS0109) and the DFG (TRR 160). This project has received funding from the European Union's Horizon 2020 research and innovation programme under the Marie Skłodowska-Curie grant agreement no. 747866 (EPPIC) and no. 753067 (OPHOCS).

## Author contributions

A.J., D.D., M.H.A. and T.S. carried out the optical experiment with input from I.S., R.J.W. and P.L. A.J., M.H.A. and S.M. performed the theory. M.C.L., I.S., A.L. and R.J.W. designed the heterostructure. R.S., A.L. and A.D.W. grew the wafer. C.P., T.P., S.S. and L.M. designed and fabricated the sample. A.J. and P.L. wrote the manuscript with input from all authors.

## Competing interests

The authors declare no competing interests.

## Additional information

**Supplementary information** is available for this paper at https://doi.org/10.1038/s41565-018-0091-5.

**Reprints and permissions information** is available at www.nature.com/reprints.

**Correspondence and requests for materials** should be addressed to A.J. or P.L.

**Publisher's note:** Springer Nature remains neutral with regard to jurisdictional claims in published maps and institutional affiliations.



© 2018 Macmillan Publishers Limited, part of Springer Nature. All rights reserved.